

Human serum albumin as protecting agent of silver nanoparticles: role of the protein conformation and amine groups in the nanoparticle stabilization

Emilio I. Alarcon · Carlos J. Bueno-Alejo ·
Christopher W. Noel · Kevin G. Stamplecoskie ·
Natalia L. Pacioni · Horacio Poblete · J. C. Scaiano

Received: 13 July 2012 / Accepted: 12 December 2012 / Published online: 1 January 2013
© Springer Science+Business Media Dordrecht 2012

Abstract Thermally denatured human serum albumin interacts with ~3.0 nm spherical AgNP enhancing the fluorescence of Trp-214 at large protein/nanoparticle ratios. However, using native HSA, no changes in the emission were observed. The observation is likely due to differences between native and denatured protein packing resulting from protein corona formation. We have also found that NH₂ blocking of the protein strongly affects the ability of the protein to protect AgNP from different salts/ions such as NaCl, PBS, Hank's buffer, Tris-HCl, MES,

and DMEM. Additionally, AgNP can be readily prepared in aqueous solutions by a photochemical approach employing HSA as an in situ protecting agent. The role of the protein in this case is beyond that of protecting agent; thus, Ag⁺ ions and I-2959 complexation within the protein structure also affects the efficiency of AgNP formation. Blocking NH₂ in HSA modified the AgNP growth profile, surface plasmon band shape, and long-term stability suggesting that amine groups are directly involved in the formation and post-stabilization of AgNP. In particular, AgNP size and shape are extensively influenced by NH₂ blocking, leading primarily to cubes and plates with sizes around 5–15 nm; in contrast, spherical monodisperse 4.0 nm AgNP are observed for native HSA. The nanoparticles prepared by this protocol are non-toxic in primary cells and have remarkable antibacterial properties. Finally, surface plasmon excitation of native HSA@AgNP promoted loss of protein conformation in just 5 min, suggesting that plasmon heating causes protein denaturation using continuous light sources such as commercial LED.

Electronic supplementary material The online version of this article (doi:10.1007/s11051-012-1374-7) contains supplementary material, which is available to authorized users.

E. I. Alarcon · C. J. Bueno-Alejo · C.W. Noel ·
K. G. Stamplecoskie · N. L. Pacioni · J. C. Scaiano (✉)
Department of Chemistry, Centre for Catalysis Research
and Innovation, University of Ottawa, 10 Marie Curie,
Ottawa, ON K1N 6N5, Canada
e-mail: tito@photo.chem.uottawa.ca

Present Address:

N. L. Pacioni
INFIQC, Departamento de Química Orgánica, Facultad de
Ciencias Químicas, Universidad Nacional de Córdoba,
Ciudad Universitaria, 5000 Cordoba, Argentina

H. Poblete
Center for Bioinformatics and Molecular Simulations,
Universidad de Talca, 2 Norte 685, Casilla 721, Talca,
Chile

Keywords Silver nanoparticles · Human serum albumin · Lysine residues · Plasmon mediated protein denaturation

Introduction

Over the last two decades, metal nanoparticles have attracted a great deal of interest for biomedical

applications. Nanotechnology has led to a wide variety of applications in the areas of catalysis, imaging, DNA-detection, and material engineering (Chatterjee et al. 2008; Elswaifi et al. 2009; Wadhwa et al. 2009; Corma and Garcia 2008; Burda et al. 2005). When evaluating the potential applications of metal nanomaterials in vivo, it is essential to determine their stability under physiological conditions. Thus, several articles have focused on the development and/or post-synthesis stabilization of biocompatible metallic nanoparticles (Swift et al. 2009; Nangia et al. 2009; Shi et al. 2007; Pattabi and Pattabi 2009; Sakai and Alexandridis 2005). The synthesis protocol for many of these materials frequently requires harsh conditions that not only decrease the overall particle yield, but also more importantly, fail to ensure metal surface protection (Varner et al. 2010; Murawala et al. 2009).

Some examples regarding the design of metallic nanoparticles stabilized with proteins have been documented in the literature (Xiao et al. 2008; Murawala et al. 2009; Eby et al. 2009). (Eby et al. 2009) for instance, have recently prepared silver nanoparticles (AgNP) functionalized with lysozyme that exhibit potent antimicrobial activity. Further, (Murawala et al. 2009) have synthesized AgNP protected with bovine serum albumin (BSA) where the BSA itself functions as the reducing agent leading to an undesired protein oxidation. Additional reports have also documented that BSA is able to interact with AgNP electrostatically (Ravindran et al. 2010; Mariam et al. 2011; De-Llanos et al. 2011) affecting the binding capacity of the protein with small molecules (De-Llanos et al. 2011). Nevertheless, research on the interaction between Human Serum Albumin (HSA), the most abundant protein in the human plasma where it can reach concentrations up to 0.6 mM (Peters 1996) and AgNP has been scarcely explored (Gebauer et al. 2012) though a deep understanding of the phenomenon is relevant for potential biomedical applications. It has also been shown that HSA can effectively interact with quantum dots and gold nanoparticles (AuNP) (Nayac and Shin 2008; Xiao et al. 2008). HSA also binds a large variety of small molecules and ions (Honore and Brodersen 1984; Pinkerton and Koeplinger 1990; Kragh-Hansen 1990; Peters 1996; Borissevitch et al. 1996; Epps et al. 1998; Alarcón et al. 2009, 2012; Aspée et al. 2009).

Despite the progress made, it remains unclear to what extent the nanoparticle presence changes protein

conformation and/or the enzymatic activity. Thus, (Bretschneider et al. 2009) have synthesized AuNP anchored to horseradish peroxidase and studied the effect of surface plasmon band (SPB) excitation on enzymatic activity. SPB excitation also provides an efficient conversion of light-to-heat that can transfer heat to the microenvironment directly around nanoparticles (Richardson et al. 2009; Fasciani et al. 2011). This local heating can promote partial protein denaturation or changes in its conformation as reported for small peptides (Slocik et al. 2007). In fact, there is a range of mechanisms by which SPB excitation can lead to physical or chemical consequences beyond the aim of the present work (Ben-Yakar et al. 2008; Scaiano et al. 2011). For protein/metallic nanoparticles hybrids, (Holland et al. 2011) recently prepared and characterized a biometallic glucose oxidase/AuNP composite where a reduction on the apparent catalytic activity of the enzyme and its K_M was observed. In particular, Silver nanoparticles (AgNP) have been explored in surface enhanced Raman scattering (SERS), catalysis, antibacterial activity, and biomedical applications (Stamplecoskie et al. 2011; Sharma et al. 2009; Suh and Moskovits 1986; Wu et al. 2008; Cinta et al. 1999; Herne et al. 1991; Li et al. 2010; Edwards-Jones 2009; Varner et al. 2010).

More specifically, we have recently observed that AgNP are unstable under physiological conditions due, to some extent, to the large ionic strength, which modifies the particle formal charge (Alarcón et al. 2012). This has not been a barrier for exploring the in vitro toxicity and antibacterial activity of AgNP (Sharma et al. 2009; Varner et al. 2010). In the present study, we have employed HSA instead of BSA as model for exploring how proteins interact with AgNP since it has been reported before the different binding capabilities of HSA and BSA in spite of their structural similarities (Harmatz et al. 1975) by manipulating the biomacromolecule conformation, and/or selectively blocking NH_2 groups we have shown that there is a combination of several non-covalent electrostatic interactions involved in such phenomenon, where NH_2 residues play a key role in the observed post-stabilization and synthesis of AgNP. We also explore to what extent SPB excitation with 405 nm LED can affect the protein conformation in the HSA@AgNP hybrid. The biocompatibility and antibacterial performance of the new nanoparticles have been also explored.

Experimental section

Chemicals

HSA (>99 %, fraction V, essentially fatty acid free) or indicated otherwise, AgNO₃, Na₂HPO₄, NaH₂PO₄, and trisodium citrate were purchased from Sigma-Aldrich. 2-Hydroxy-1-[4-(2-hydroxyethoxy)phenyl]-2-methyl-1-propanone (I-2959) was a generous gift from Ciba Specialty Chemicals; Sulfo-NHS acetate was purchased from Thermo Scientific; PD-10 desalting columns were obtained from GE Healthcare. Stability experiments were carried out in saline phosphate buffer solution (PBS 100 mM at pH 7.4), Hanks buffer (HBBS at pH 7.0), Dulbecco's modified eagle medium (DMEM), and tris(hydroxymethyl)aminomethane buffer (Tris 0.1 M at pH 9.0). NaCl solutions were prepared using Milli-Q water. The effect of pH solution on the HSA stabilizer ability was determined using 2-(N-morpholino)ethanesulfonic (MES) buffer (0.6 M) at pH 5.0 or 7.0. The stability of HSA@AgNP and citrate protected AgNP was assessed by incubating the nanoparticles in simulated body fluid (SBF) at 37 °C and monitoring their plasmonic absorption for up to 48 h.

Absorption spectra

Absorbance spectra were recorded using a Cary-100-Bio UV-Vis spectrophotometer (Varian) employing 0.7 cm pathlength cuvettes. All the spectra were recorded using a scan speed of 500 nm/min at room temperature.

Fluorescence emission spectra

Quenching of tryptophan-214 (Trp) fluorescence in HSA was monitored as previously described (Alarcón et al. 2010; Garcia et al. 2011). Protein solutions were kept in dark for at least an hour before measurements, and their concentrations were adjusted using $\epsilon = 35,353 \text{ /cm}^{-1}\text{M}^{-1}$ at 280 nm (Raymond et al. 1967). Fluorescence spectra for HSA were recorded using a PTI spectrofluorimeter employing 1.0 cm pathlength cuvettes. All spectra were recorded using 295 nm excitation and scanned from 305 to 600 nm at room temperature; protein absorbance was kept below 0.2. Inner filter effect correction by AgNP addition

was applied in all cases as described by Kubista et al. (1994).

Effect of HSA on AgNP stability

The stability of AgNP was evaluated in the presence of either different NaCl concentrations, buffers such as PBS, HBBS, and DMEM. AgNP stability was determined by measuring the absorption spectrum of a mixture of AgNP (6 nM) and NaCl (150 mM) or buffer (at different concentrations). The measurements were carried out at different incubation times (from 0 to 18 h) and temperatures in a 96-well plate in a SpectraMax 5 from Molecular Devices.

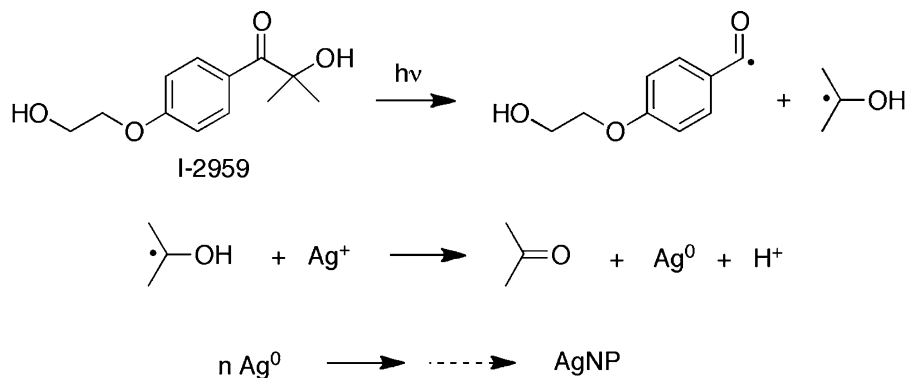
Synthesis of AgNP and HSA@AgNP

AgNP were prepared from deoxygenated (30 min) 0.2 mM AgNO₃, 0.2 mM I-2959, and 1.0 mM sodium citrate irradiated with UVA light (8 lamps, in a Luzchem CCP-4 V photoreactor at 25.0 ± 0.5 °C). A similar procedure was used for preparing HSA-coated AgNP (HSA@AgNP) but in this case sodium citrate was replaced by micromolar concentrations of HSA. Our approach is based on the Norrish Type I photocleavage of I-2959 leading to ketyl radicals with a quantum efficiency of 0.29 (Jockusch et al. 2001). Silver cations, Ag⁺, scavenge the (CH₃)₂C[•]OH radical (ketyl) and reduce Ag⁺ to Ag⁰ (see Scheme 1) (Stamplecoskie and Scaiano 2010; Scaiano et al. 2011; Scaiano et al. 2006).

Blockage of NH₂ groups in HSA

A solution of 10 mg of HSA (75 μM) in 2.0 mL of PBS was treated with 10 mg of sulfo-NHS acetate and allowed to react at room temperature for 1 h in the dark. The treated HSA was then purified using a pre-packaged desalting Sephadex column (PD-10 Columns, GE Healthcare UK CAS 17-0851-01). GE's gravity protocol was performed as described by GE Healthcare. The eluent was then lyophilized and reconstituted to make a solution of the desired concentration. In all cases protein content in the powder was determined using BCA Bio-Rad protein assay kit using bovine serum albumin (99 %) as standard (Smith et al. 1985). The degree of NH₂ blockage was determined by MALDI-TOF analysis performed in a Bruker Microflex LT instrument using

Scheme 1 Overall reaction for the formation of silver nanoparticles. Sodium citrate (a stabilizer) has been omitted from this scheme



sinapic acid as the matrix and an MSP96 polished steel target. For the analysis 1.0 μL of a 50:50 solution of the matrix (saturated) and HSA solution (10 μM) were placed on the target. MALDI-TOF spectra for Native and blocked HSA are shown in the supporting information Figure S1 and S2, respectively. From the difference on the molecular weight obtained an average of 18 NH_2 blocked residues were determined.

Protein conformation changes after NH_2 blocking or plasmon band excitation

Circular dichroism (CD) measurements were carried out with a Jasco J-810 spectropolarimeter equipped with a 150 W xenon lamp (1.0 nm data pitch, continuous scanning mode, 50 nm/min scan speed, 0.125 s response, and 2 nm bandwidth). The conformational changes were expressed as the loss of CD signal at 222 nm. All the measurements were performed in a 0.1 cm pathlength quartz cell. The CD spectra were recorded at different irradiation times from 0 to 5 min in 100 mM phosphate buffer. CD measurements for native and blocked HSA do not reveal any significant change in the protein conformation as shown in Figure S3. This result is in line with the selective modification of the most solvent-exposed NH_2 residues in the protein as shown in Figure S4 (see next section for more details).

Computational simulation of solvent-exposed NH_2 residues in HSA

The images of human serum albumin free fatty acids (protein data bank code: 1e78) were obtained using a visual molecular dynamic (VMD) software (Humphrey et al. 1996). The surface was represented using New Cartoon representation in VMD. Lys, Arg, and Asn

residues were separately highlighted in the figures (see supporting information Figure S4 for more details).

LED excitation of the surface plasmon band

The experimental setup for LED irradiations is the same as that employed in a previous work (Stamplecoskie and Scaiano 2010). Briefly, the 405 nm LED were purchased from Roithner Lasertechnik and the home made setup used four cooled LED units, aimed at a cuvette (see Figure S5).

TEM images, dynamic light scattering, and zeta potential measurements

Samples for electron microscopy were prepared by delivering $\sim 10 \mu\text{L}$ of solution to carbon-coated copper grids (400 mesh) and dried in a vacuum system. Electron microscopy images were obtained using a JSM-7500F FESEM from JEOL Inc operating in the transmission mode (TEM). The zeta potential and hydrodynamic sizes were measured using a dynamic light scattering Malvern Zetasizer Nano ZS (Note: the pH of all the solutions was approximately 7.4).

HSA thermal denaturation

A 100 μM aqueous solution of HSA was placed in a thermal bath at 95 $^\circ\text{C}$ for 10 min and then refrigerated at 4–8 $^\circ\text{C}$ to accelerate cooling.

Biocompatibility and antibacterial performance of AgNP and HSA@AgNP

The cytotoxicity of AgNP and HSA@AgNP was evaluated in vitro using human primary dermal

fibroblast (ATCC, USA) at passage numbers lower than five. The fibroblasts were grown in Dulbecco's modified eagle's medium (DMEM, Gibco) containing 10 % fetal calf serum and 1.0 % penicillin/streptomycin, and cultured at 37 °C, 5.0 % CO₂, and 100 % humidity. Cell viability was evaluated using CellTiter 96[®] Aqueous MTS colorimetric viability assay (Promega) and employed as a measure of cell survival after 6, 24, and 48 h of incubation. Briefly, from confluent fibroblasts cultured, 5×10^4 cell/mL were seeded in a 96-well plate followed by overnight incubation, prior to addition of nanoparticles or AgNO₃. The samples were incubated for different times 6, 24, or 48 h and the well contents were replaced by 100 μ L fresh cell culture medium, and 20 μ L of MTS solution added and incubated for 2 h and the absorbance at 490 nm measured in a 96-well plate in a SpectraMax 5 from Molecular Devices. Viable cell density was determined by interpolation of the 490 nm absorption in a calibration curve of MTS at different cell densities as seen in Figure S10.

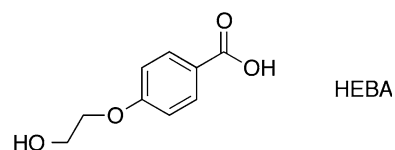
The antimicrobial activity of the AgNP, HSA@AgNP, and AgNO₃ were assessed against the gram (-) mutant kanamycin and tetracycline resistant bacteria *Escherichia coli* (BRL2). Growth inhibition was carried out following standard protocols as described in the standard Clinical and Laboratory Standards Institute (CLSI) protocol (Wikler 2005). Exponentially growing cultures were incubated at 37 °C with or without AgNP or AgNO₃ for 24 h in 96-well plates (Falcon[™]) at a bacteria density of $\approx 1.0 \times 10^5$ cfu/mL in 25 % Lysogeny broth (LB). Bacteria growth was monitored in a SpectraMax 5 from Molecular Devices as the optical density at 600 nm (OD₆₀₀) in each well (see Figure S11).

Results and discussion

Stabilization of AgNP by HSA

AgNP were prepared as indicated above (see Scheme 1). In contrast with AuNP (McGilvray et al. 2006; Marin et al. 2008) this reaction must be performed in the presence of a stabilizing agent since unprotected AgNP are not stable in pure water (Stamplecoskie and Scaiano 2010). Addition of 3.0 nm AgNP prepared as above (~ 25 nM, stock solution) into native or denatured 10 μ M HSA in water

(see Fig. 1A, B) causes a change in the protein fluorescence only in the case of denatured HSA. Data from denatured HSA (Fig. 1B, C) show an enhancement region for the Trp intrinsic fluorescence at AgNP < 0.38 nM (see Fig. 1B) while at concentrations higher than 2.0 nM there is almost no measurable quenching under our experimental detection limit. In all cases no modification of the Trp fluorescence lifetime was detected (data not shown) indicative of a static quenching mechanism. Control experiments with Ag⁺, I-2959, or HEBA showed only minor emission changes at similar concentrations as employed in the quenching by AgNP (see Table 1). HEBA is a known oxidation product of the substituted benzoyl radical (Scheme 1).



The bimodal behavior in the fluorescence of denatured HSA can be explained by the formation of protein corona arrangements (Lynch and Dawson 2008) that at AgNP concentrations lower than 0.38 nM leads to a marked emission enhancement as they locate in the plasmon enhancement region. This enhanced emission becomes a smaller fraction of the total emission as the concentration of AgNP increases due to the finite availability of nanoparticle surface. Effectively, the ratio of HSA/AgNP at the maximum enhancement shown in Fig. 1B is close to 160,000 molecules per AgNP, while at AgNP concentrations > 0.5 nM this will be less than 16,000 molecules per AgNP. These data are fully compatible with the formation of corona arrangement where there is a considerable excess of “free protein” in the aqueous phase. This corona arrangement is obviously different from the one formed for the native protein since no effect on the fluorescence emission was observed for the non-denatured protein as displayed in Fig. 1C; the changes for denatured HSA, while modest (~ 20 %) are outside error limits and are not observed for the native protein. The most likely explanation is that the formation of an initial shell of the unfolded HSA surrounding the metal surface facilitates the sequential association of more denatured protein. However, in the case of native HSA

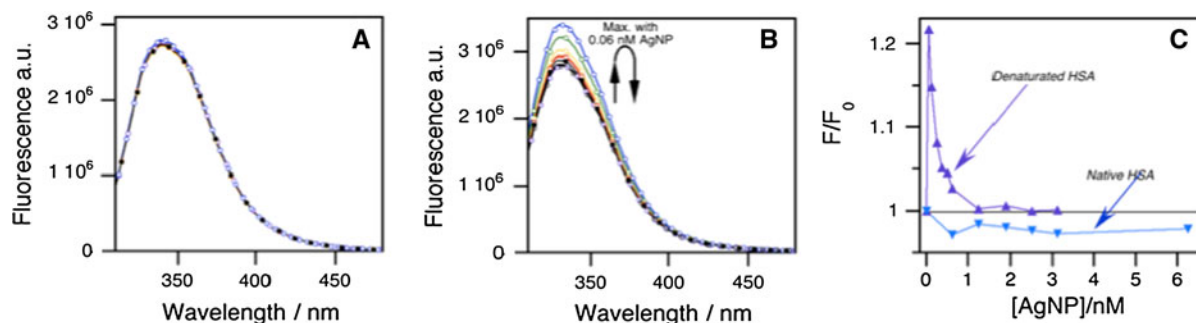


Fig. 1 Effect of AgNP addition in Trp-214 HSA fluorescence. Representative plots displaying the changes in the 10 μ M protein emissions the nanoparticle concentration increases from 0 (red line) to 6.25 nM (bold black line) for native (A) or heat-treated (B) human serum albumin. Changes in fluorescence

intensity ($\lambda_{exc} = 295$ nm) expressed as F/F_0 for denatured ($\lambda_{em} = 332$ nm) and native ($\lambda_{em} = 340$ nm) protein in the presence of increasing concentration of AgNP (C). All measurements were done by triplicate, in three different days at room temperature

Table 1 Native HSA fluorescence quenching parameters for the different compounds present in AgNP aqueous solution

Compound	$K_{SV}/10^2$ (M^{-1})
AgNO ₃	1.10
Citrate	<0.4
I-2959	5.0 ^a
HEBA	2.0

K_{SV} is the Stern–Volmer constant for the quenching process

^a Value determined from the initial slope after inner filter correction

it is not possible to form such layer because the rigid geometry of the protein resembles a rectangle of $3.0 \times 8.0 \times 8.0$ nm, (Peters 1996) that precludes other protein molecules from approaching enough to cause a fluorescence enhancement.

We believe that there must be three populations for the proteins: (i) protein directly bound to the AgNP surface, (ii) a protein shell in close contact with the first “contact” protein layer, and (iii) free protein in the aqueous phase. The three populations must be in dynamic equilibrium. Circular dichroism experiments in the presence of AgNP did not show any significant modification in the protein conformation, suggesting that only a small population of HSA is directly bound to the metallic surface (data not shown). Attempts to measure thermodynamic parameters for the formation of this corona arrangement were carried out by Isothermal titration calorimetry. However, no reliable data was obtained most likely due to limitations with the resolution limit of our equipment.

We wondered if it was possible for such protein supramolecular organization to improve the stability

of the nanoparticle under physiological conditions. This point is of great interest, since AgNP are easily degraded in the presence of chloride ions, available at ~ 150 mM in living organisms. Figure 2 displays the effect of different protein concentrations on the absorption spectra of AgNP in aqueous 150 mM NaCl.

Figure 2A (inset) shows that the plasmonic absorbance from AgNP fades in the presence of NaCl 150 mM and a new broad band appears between 500 and 700 nm. This is attributed to AgNP aggregation promoted by chloride ions. This can be prevented by addition of >0.05 μ M protein (Fig. 2B). Thus, assuming a AgNP concentration of 25 nM, at least two HSA molecules are required to protect each AgNP. When the protein concentration exceeds 100 μ M a decrease in the SPB intensity was observed (zone II in Fig. 2A); we hypothesize that protein aggregation is favoured at concentrations > 100 μ M (Peters 1996) thus decreasing the protection conferred by monomeric HSA. We postulate that this protecting effect depends on the number of available NH₂ groups, rather than the macromolecule conformation, as suggested by Fig. 2B. These data suggest that electrostatic interactions confer protection to the AgNP surface (Lynch and Dawson 2008). Additionally, we have observed that protein protection against NaCl, and other salts, was not significantly affected by the presence of (≤ 0.5 mM) sodium citrate, I-2959, or HEBA (data not shown). This indicates that these components are not involved in the formation of the corona arrangement. Recognizing that NaCl is not the only substance that can potentially decrease the AgNP stability, we also assessed their stability with different buffers such as,

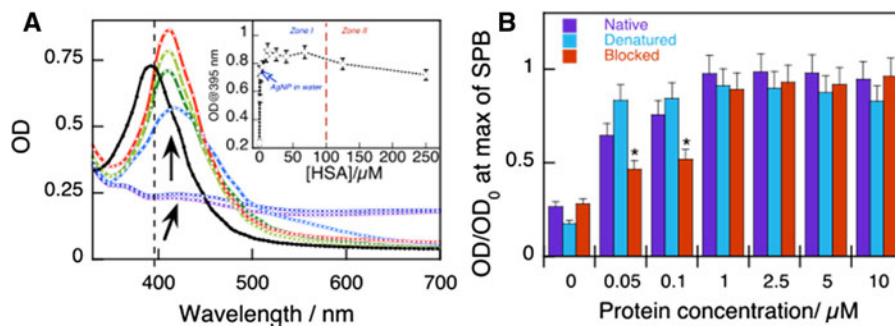


Fig. 2 **A** Effect of HSA concentration on plasmonic absorption in aqueous ~ 25 nM AgNP and 150 mM NaCl: 0 μM (purple circles), 0.01 μM (blue circles), 1.0 μM (light blue circles), 2.5 μM (green circles), 5.0 μM (light green circles), and 10 μM (red circles). The absorption spectrum for AgNP at the same concentration in water is also included (black circles). The dashed line indicates the position of 395 nm in the plot. **B** Changes in the AgNP SPB maximum in 150 mM NaCl solutions containing different kinds of HSA (native, denatured,

phosphate buffer saline (PBS 100 mM, pH 7.0), glucose supplemented phosphate buffer (Hank's buffer), Dulbecco's minimum media (DMEM) buffer (buffer-formulation commonly employed in cell culturing), MES buffer (600 mM, pH 7.0), and Tris-HCl buffer (100 mM, pH 7.0). Figure 3A–C shows that even at low protein concentrations (0.2 μM) AgNP become stable in all the buffers assessed, with a concomitant SPB red shift of ~ 8.0 nm. Remarkably, as the buffer complexity increases, the protein protection efficacy seems to decrease. In particular, the minimum protein concentration needed for conferring protection to AgNP becomes greater as the number of components in the buffer increases (DMEM > Hank's buffer > phosphate buffer saline). The most noteworthy difference within the buffers was found in the 18 h stability experiments (Fig. 3D) for DMEM; where AgNP SPB clearly decreases after only 3 h, probably due to protein oxidation promoted by the components in the medium (aminoacids, vitamins, minerals, etc.). Protein protection was also observed for AgNP in Tris-HCl buffer and to a lesser extent if MES buffer is employed as shown in Figure S6.

Synthesis and characterization of HSA-coated silver nanostructures

In an attempt to obtain biocompatible AgNP, we initially attempted the I-2959 mediated photochemical synthesis of AgNP using the free L-amino acids Trp,

and amine group-blocked) with concentration ranging from 0 to 10 μM . Asterisks in **B** indicate AgNP spontaneous aggregation. Inset in **A** shows the changes in the absorption at 395 nm as function of native HSA concentration in a wider concentration range. The data measured for AgNP in water are identified with a blue arrow. All measurements performed at room temperature; the error bars in inset **A** correspond to the average of three independent measurements. In **B** 10 % error bars have been added

Tyr, Met, Lys, His, and Cys as stabilizing agents. However, no nanoparticles were obtained using this approach (data not shown). Next we tested HSA as protecting agent. Figure 4 shows the AgNP absorption spectra obtained using citrate 1.0 mM and/or different HSA concentrations, from 0.3 to 1.2 μM , upon 15 min UVA irradiation. Control experiments irradiating HSA and silver nitrate solution did not produce any AgNP. A red shift on SPB from 385 ± 3.0 to 397 ± 2.0 nm is observed immediately after AgNP synthesis in the presence of HSA. Similar results have been described for other metallic nanoparticles synthesized employing polymers and/or biomolecules as stabilizing agents (Nayac and Shin 2008; Murawala et al. 2009; Nangia et al. 2009; Pattabi and Pattabi 2009).

We note that the SPB growth rate, determined as the area under the curve for HSA@AgNP (see Figure S7), and citrate stabilized AgNP showed different profiles suggesting differences during the AgNP growth processes. Given that the absorbance of I-2959 is very similar in all the systems, we concluded that HSA interferes with either the photochemistry of I-2959, or with the ketyl radical reaction leading to Ag^+ reduction. Experiments using different I-2959 concentrations (0.1, 0.2, and 0.3 mM) in the presence of constant native HSA (1.2 μM) revealed that the growth is faster at higher I-2959 concentrations, as expected, given the increase in radical formation rate. In contrast, when maintaining a fixed I-2959

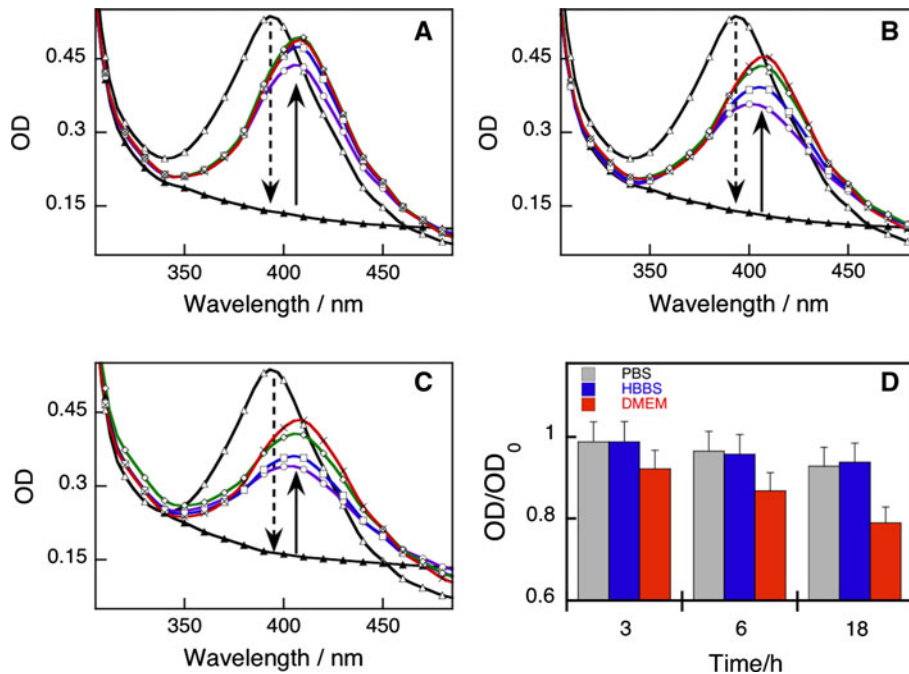


Fig. 3 Effect of HSA on AgNP SPB absorption in different buffers; phosphate buffer saline (**A**), Hank's buffer (**B**), and DMEM (**C**). Spectra taken at different protein concentrations: 0 μM (black filled triangles), 0.2 μM (purple circles), 1.0 μM (blue squares), 2.0 μM (green diamonds), and 5.0 μM (red X); the aqueous absorption spectrum of AgNP has been also included for comparison (black open triangles). The arrows in **A–C** denote SPB changes (OD_0 corresponds to the optical

concentration (0.2 mM) and changing the native HSA concentration from 0.6 to 4.8 μM , the results show that when the protein concentration increases, the growth rate for the SPB decreases. Figure 5 illustrates this effect; extrapolation of the data in the inset suggests that protein-protected I-2959 generates the SPB at only one third of the rate observed when the protein is absent.

We have also noted (see Figure S7) that the presence of native HSA decreases the AgNP formation rate as compared to citrate protected AgNP. Further, after only ~ 5.0 min a plateau is reached which most likely corresponds to the completed reduction of Ag^+ to Ag^0 . Given that the integrated area under the SPB spectra is slightly larger when HSA is present, this suggests that the photochemistry of I-2959 has a reduced quantum yield when incorporated in HSA. The SPB growth was slower for NH_2 -blocked HSA compared with native HSA.

The zeta potential (ζ) and hydrodynamic size (HDS) were measured for all the AgNP and proteins.

density at the maximum at time zero). **D** AgNP stability evaluated at 395 nm in the three different buffers using 5.0 μM HSA after 3, 6, and 18 h incubation. All measurements were carried out at room temperature by quadruplicate; errors were $<5.0\%$ in all cases (5 % error bars have been included in the plot). Similar plots for the remaining buffers are included in the supporting information (Figure S6)

Figure 6 shows that values of ζ change from -33 ± 2.0 to -56 ± 3.0 mV after NH_2 blocking of HSA. Differences are likely due to the reduced total number of available NH_2 after blocking (roughly 18 NH_2 groups blocked). Interestingly, when native HSA is used as the stabilizing agent, ζ changed from -49 ± 2.0 to $+41 \pm 3.0$ mV. This is in line with the expected surface protection by the macromolecule where its arrangement on the metallic surface through non-covalent interactions leads to ζ modification. The role of ionizable carboxylic acids was also explored; however, the current protocols for blocking carboxylic acids required several steps and harsh conditions, when compared to NH_2 blocking.

The long-term stability for the AgNP prepared using either HSA and NH_2 -blocked HSA are shown in Fig. 7 plotted as the AUC (350–550 nm) for each AgNP SPB at different times after synthesis for up to 120 h. Figure 7 shows that neither for citrate@AgNP nor for HSA@AgNP the AUC changed significantly after 120 h. In fact, we have observed a remarkable

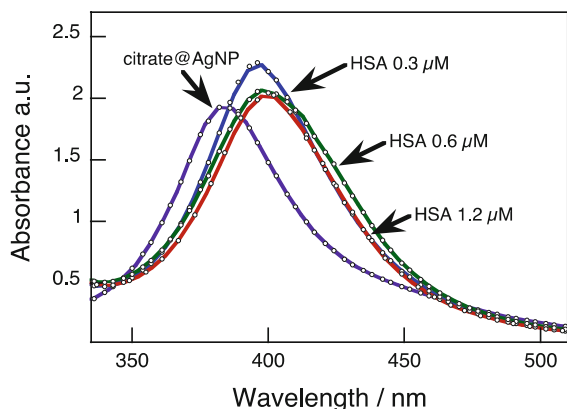


Fig. 4 Absorption spectra for colloidal AgNP after 15 min irradiation prepared using as stabilizers citrate or HSA at different concentration: 0.3 μM , 0.6 μM , and 1.2 μM ; I-2959 was 0.2 mM. All measurements performed at 25.0 ± 0.5 °C in aqueous solutions using eight UVA lamps

stability for both kinds of particles over the course of a month. In contrast, NH_2 -blocked HSA were no longer stable after 24 h, particularly the sample prepared using 0.3 μM of NH_2 -blocked HSA that spontaneously aggregated after this time; more importantly, even at higher concentrations the SPB decayed steadily indicating poor nanoparticle stability. Changes on AgNP SPB maximum for all the nanoparticles were also detected. The strongest change occurs for citrate@AgNP, where SPB is 23 nm red shifted after 24 h from its original value after synthesis (375 nm). This value was maintained constant up to 120 h as shown in Fig. 7. These changes are probably related to a post-synthesis AgNP growth (ripening) in the first 24 h. For both HSA types the red shift was close to 15 nm.

Even though this provoked an important loss in alpha helix content, we found that its role in the stabilization and synthesis of AgNP is very similar to that provided by native HSA (data not shown). Moreover, we consider that a model involving primarily NH_2 explains consistently the observed behavior. As the data for HSA shows that concentrations below 0.3 μM are enough to stabilize AgNP (25 nM using 5.2 ± 0.1 nm AgNP from SEM (see Figure S8) there must be around 4.0 protein molecules stabilizing each AgNP.

The AgNP with NH_2 -blocked HSA have ζ values smaller than those obtained with native HSA. These values point to a reduced colloidal stability for NH_2 -blocked HSA. The particles prepared using NH_2 -

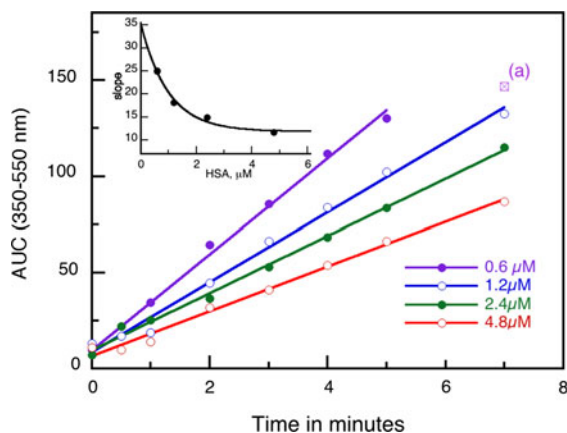


Fig. 5 Effect of different native HSA concentrations on the SPB growth in the presence of constant I-2959 (0.2 mM) and constant Ag^+ (0.2 mM); it shows a slower growth as the HSA concentration increases. All datasets approximated with a linear fit; the point marked (a) belongs to the 0.6 μM dataset, but was not used for the fit because it shows saturation (as expected as high Ag^+ conversion). The inset shows the slope as a function of HSA concentration

blocked HSA are considerably bigger 30–1140 nm, than their HSA@AgNP counterpart (8.5 nm average size), an observation that is consistent with their reduced stability. These results cannot be explained by differences in either HSA conformation or size (similar HDS were measured for both HSA and NH_2 -blocked HSA). The most probable explanation is that differences in growth mechanisms conferred reduced stability to nascent particles when NH_2 -blocked HSA is used. This is supported by electron microscopy images (see Figure S8) where the formation of cubes, rods, and plates (apart from small-sized spherical AgNP) takes place with NH_2 -blocked HSA. The presence of cubic structures with absorption maxima at 420 nm (Stamplecoskie and Scaiano 2010; McEachran and Kitaev 2008) bears great resemblance to the crystalline structure of HSA that coincidentally possesses such of crystalline arrangement in the solid state (Murawala et al. 2009). Interestingly, as NH_2 -HSA@AgNP are gradually formed it promotes (see Figure S8) crystallization and the formation of some cubic structures. The simplicity of our approach compares well with the few reported synthetic routes for silver cubes (Sun and Xia 2002; Tran et al. 2008; Murphy et al. 2005; McEachran and Kitaev 2008).

The stability of our new HSA@AgNP in simulated body fluid was also assessed as seen in Figure S9. This figure shows how only HSA protected silver

Fig. 6 Zeta potential **A** left and hydrodynamic sizes **B** right for citrate@AgNP (labeled as citrate) and AgNP prepared using different concentrations of either native or NH₂-blocked HSA measured 24 h after AgNP synthesis. Control experiments with native protein or NH₂-blocked HSA have been also included in the plot. The error bars correspond to the SD from four independent measurements at 25 °C

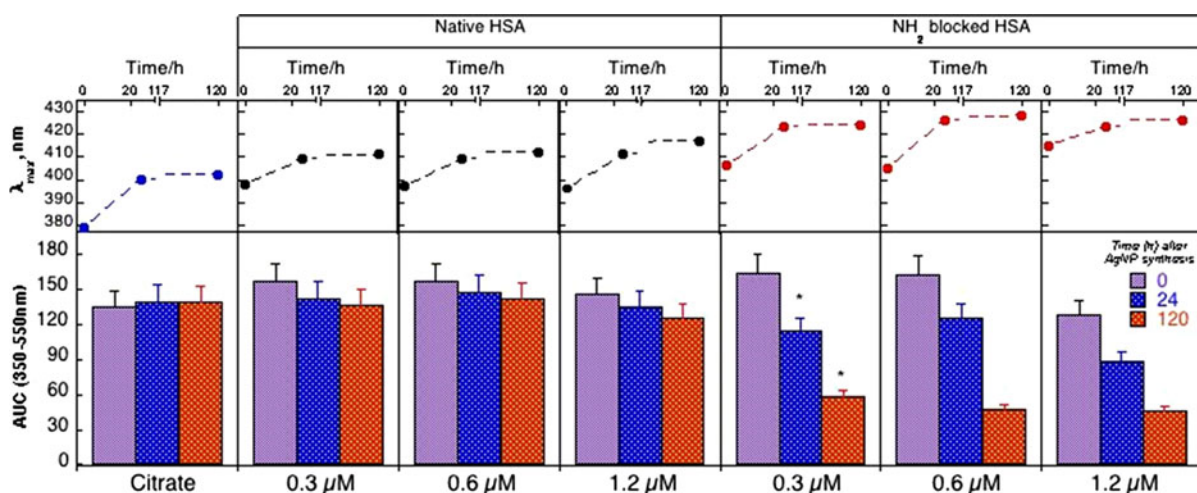
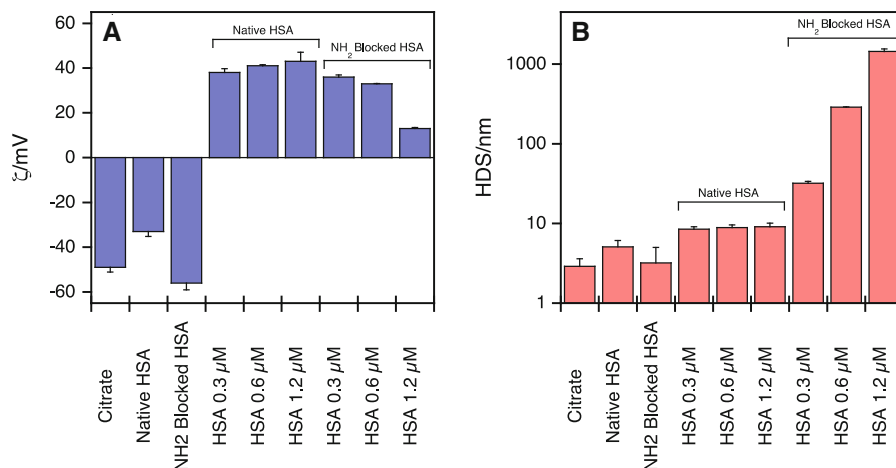


Fig. 7 Bottom changes in SPB absorption area under the curve (between 350 and 550 nm) for citrate@AgNP (citrate), native and amine-blocked HSA, prepared using different protein concentrations as shown in the bottom of x-axis, measured at 0 h (violet bars), 24 h (blue bars), and 120 h (red bars) after AgNP synthesis (15 min UVA irradiation). Top variation on

AgNP surface plasmon band position after 0, 24, and 120 h (top x-axis) nanoparticle synthesis; a break in the x-axis has been included between 30 and 117 h to facilitate plot understanding. The asterisks on the bottom figure indicate nanoparticle aggregation. An approximated 10 % error has been added to the bar plots

nanoparticles were stable in the SBF solution for up to 48 h, SPB decreases only 20 %, in comparison to the spontaneous aggregation observed for citrate@AgNP. With this in mind the biocompatibility of HSA@AgNP on human fibroblasts was also evaluated. Figure S10 summarizes the cell viability measured after different incubation times, from 6 to 48 h, for skin fibroblasts in the presence of HSA@AgNP, citrate@AgNP, or AgNO₃. The salt precursor, AgNO₃, seems to be extremely toxic at concentrations higher than 30 μM, meanwhile concentrations between 15 and 30 μM affect cell proliferation.

HSA@AgNP and citrate@AgNP, on the other hand, do not exhibit either any toxicity or affect cell proliferation indicating a good biocompatibility of these nanoparticles on primary cells. In the particular case of citrate@AgNP we believe the presence of fetal calf serum in the cell culture medium helps to decrease their toxicity by preventing the nanoparticle aggregation, leading the formation of the proven toxic ionic silver.

The antibacterial performance of our nanoparticles was also assessed and compared with AgNO₃. This time we have chosen an antibiotic resistant bacteria

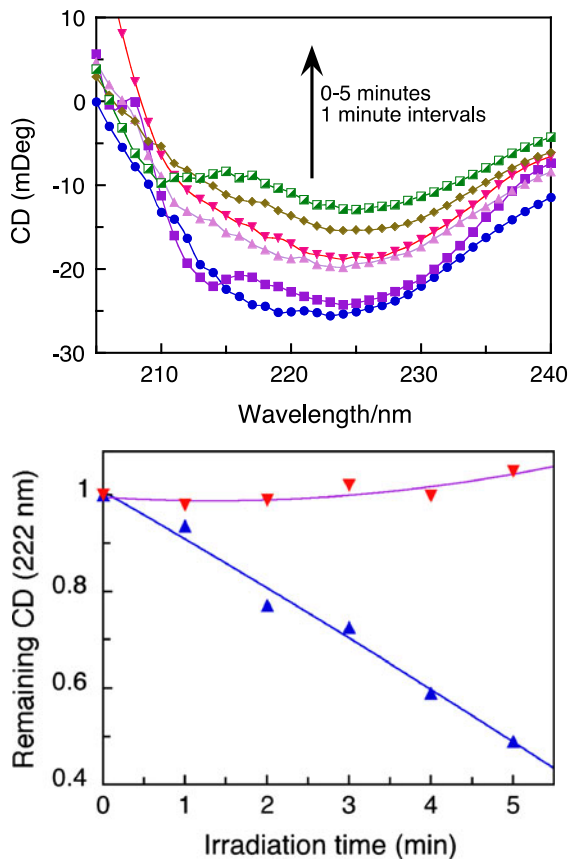


Fig. 8 Effect of the irradiation (at 405 nm) on the circular dichroism (CD) spectra of HSA@AgNP (1.2 μM protein). *Top* CD spectra as a function of irradiation time up to 5 min (indicated by the arrow). *Bottom* change in the CD signal at 222 nm expressed as remaining percentage for HSA@AgNP (small blue diamond) or free HSA 1.0 μM (big red diamond), as function of the irradiation time. All measurements in 100 mM phosphate buffer at pH 7.4

strand *E. Coli* (see experimental) and growth inhibition experiments were carried out. In the particular case of HSA@AgNP we did observe a delay in the bacteria growth as the concentration of the nanoparticle increases as seen in Figure S11. In this Figure we have also included the OD at 600 nm measured after 24 h incubation with the bacteria, and it is seen that both nanoparticles, citrate and HSA protected AgNP, have similar performance as antibacterial agents but only the HSA composite was stable, non-aggregate, in the LB medium. Note that HSA@AgNP could be potentially used at concentrations of 50 μM, total silver, or 6.25 nM nanoparticle concentrations as antibacterial agent because it is not toxic, see Figure S10, as compared to AgNO₃.

HSA denaturation upon AgNP SPB excitation

Excitation of SPB transitions leads to highly efficient light-to-heat conversion (Dulkeith et al. 2004; Richardson et al. 2009; Scaiano et al. 2011). The extreme local heat has been proposed as alternative treatment for Alzheimer diseases (β-amyloid disruption) (Triulzi et al. 2008; Kogan et al. 2006) and hyperthermia cancer therapy (Cheong et al. 2009; Cherukuri et al. 2010). The efficiency of the processes depends on the protein-nanoparticle interaction, native protein stability, and particle heat dissipation. We have examined the effect of 405 nm irradiation on HSA@AgNP. The results are shown in Fig. 8. It is important to note that HSA protein conformation (taking into account the specific protein rotation at 222 nm in CD) following AgNP preparation was almost 40 % lower than their native conformation, reflecting that protein conformation is preserved to an important extent during nanoparticle synthesis. This could signify a probable loss of helix content when HSA is bound to the metal surface. Similar observations have been described by Murawala et al. (2009) using bovine serum albumin in the preparation of AgNP.

Conclusions

Thermally denatured HSA interacts with ~3.0 nm spherical citrate protected AgNP leading to an enhancement of the fluorescence emission of the Trp-214, most likely located within the plasmon enhancement region of the nanoparticle. Formation of protein corona is the most likely explanation for this phenomenon.

The effectiveness of native HSA as a stabilizer for AgNP was also demonstrated by the changes on the SPB absorption upon protein addition. The red shift of SPB in the presence of HSA is a clear indication of dielectric constant changes at the nanoparticle surface. Further, AgNP are unstable in the presence of chloride ions. Surprisingly, we have found that even relatively low concentrations of HSA can protect citrate@AgNP from different salts/ions such as NaCl or common buffers. Nevertheless, long-term stability for AgNP conferred by HSA is apparently controlled by the medium complexity where an increase in the number of components in the buffer cause the particles to be less stable.

We also noted that the protecting efficiency of HSA is strongly influenced by the availability of NH_2 groups rather than the macromolecule conformation. Further, the solution pH, in MES buffer pH 5.0 or 7.0, seems to also affect the protection capacity of the protein due to a change in protonation state.

Silver nanoparticles can be readily prepared in aqueous solutions under mild conditions using a photochemical method with HSA as protecting agent. The protein is more than just a mere protecting agent, since it could also complex Ag^+ ions and affect the ratio of Ag^+ between the aqueous solution and the macromolecule structure as HSA shows a remarkable affinity for silver ions. Long-term stability experiments have shown that amine-blocked HSA are far less stable than when using native HSA or even the protein alone. The hydrodynamic size measurements for the nanoparticles showed that the nanocomposite size is highly modified when the NH_2 groups in HSA are blocked. It is also of note that when NH_2 -blocked HSA is employed as a stabilizer, in the presence of other AgNP shapes (primarily cubes and plates) and sizes (5–15 nm), these are different from those obtained using native HSA. The HSA@AgNP composites shown to be stable in physiological simulated medium and non-toxic in primary cell cultures of skin fibroblasts. They also have antibacterial properties similar to the observed for citrate@AgNP but with improved stability.

Surface plasmon excitation of HSA@AgNP promoted loss of conformation of bound protein within 5 min, suggesting that plasmon heating can readily induce protein denaturation using continuous light sources such as LED. Our own work shows that local temperatures as high 500 °C can be reached for submicrosecond times (with AuNP) although this high temperature is only reached in the near vicinity of the nanoparticle and its effect on the bulk solution is minor.

Our work provides another example where new biocompatible nanomaterials can be made in a facile one-step reaction. By understanding the interactions between biomolecules and metallic nanoparticles it may be possible to manipulate them in order to produce a variety of silver nanostructures that can be selectively prepared and then be delivered to pre-selected organs or biocomponents and triggered photochemically with spatial and temporal control.

Acknowledgments This work was supported by the Natural Sciences and Engineering Research Council of Canada. We thank Michel Grenier who designed the LED irradiation system, as well as for his support in laser flash photolysis measurements. EIA. thanks Becas Chile for Post-Doctoral support. HP thanks the Programa de Doctorado en Ciencias Aplicadas at Universidad de Talca, Chile for financial support. We would like to thank Prof. Christopher Boddy, University of Ottawa, for providing the bacterial strand employed in this work.

References

- Alarcon E, Aspee A, Abuin EB, Lissi EA (2012) Evaluation of solute binding to proteins and intra-protein distances from steady state fluorescence measurements. *J Photochem Photobiol B* 106(1):1–17. doi:[10.1016/j.jphotobiol.2011.11.002](https://doi.org/10.1016/j.jphotobiol.2011.11.002)
- Alarcón E, Edwards AM, Garcia AM, Muñoz M, Aspée A, Borsarelli CD, Lissi EA (2009) Photophysics and photochemistry of zinc phthalocyanine/bovine serum albumin adducts. *Photochem Photobiol Sci* 8(2):255–263. doi:[10.1039/B815726J](https://doi.org/10.1039/B815726J)
- Alarcón E, Edwards AM, Aspée A, Gonzalez-Nilo D, Moran FE, Borsarelli CD, Lissi EA, Poblete H, Scaiano JC (2010) Photophysics and photochemistry of dyes bound to human serum albumin are determined by the dye localization. *Photochem Photobiol Sci* 9(1):93–102. doi:[10.1039/B9PP00091G](https://doi.org/10.1039/B9PP00091G)
- Alarcón E, Udekwi K, Skog M, Pacioni NL, Stamplecoskie KL, Gonzalez-Béjar M, Polisetti N, Wickham A, Richter-Dahlfors A, Griffith M, Scaiano JC (2012) The biocompatibility and antibacterial properties of collagen-stabilized, photochemically prepared silver nanoparticles. *Biomaterials* 33(19):4947–4956. doi:[10.1016/j.biomaterials.2012.03.033](https://doi.org/10.1016/j.biomaterials.2012.03.033)
- Aspée A, Orrego A, Alarcón E, Alarcón CL, Poblete H, González-Nilo D (2009) Antioxidant reactivity towards nitroxide probes anchored into human serum albumin. A new model for studying antioxidant repairing capacity of protein radicals. *Bioorg Med Chem Lett* 19(22):6382–6385. doi:[10.1016/j.bmcl.2009.09.070](https://doi.org/10.1016/j.bmcl.2009.09.070)
- Ben-Yakar A, Eversole D, Ekici O (2008) Spherical and anisotropic gold nanoparticles in plasmonic laser phototherapy of cancer. In: Kumar C (ed) *Non-magnetic metallic nanomaterials for life science*, vol 10, nanomaterials for life sciences. Wiley, Weinheim, pp 493–539
- Borissevitch IE, Tominaga TT, Imasato H, Tabak M (1996) Fluorescence and optical absorption study of interaction of two water soluble porphyrins with bovine serum albumin. The role of albumin and porphyrin aggregation. *J Lumin* 69(2):65–76. doi:[10.1016/0022-2313\(96\)00037-3](https://doi.org/10.1016/0022-2313(96)00037-3)
- Bretschneider JC, Reismann M, Von Plessen G, Simon U (2009) Photothermal control of the activity of HRP-functionalized gold nanoparticles. *Small* 5(22):2549–2553. doi:[10.1002/smll.200900544](https://doi.org/10.1002/smll.200900544)
- Burda C, Chen X, Narayanan R, El-Sayed MA (2005) Chemistry and properties of nanocrystals of different shapes. *Chem Rev* 105(4):1025–1102. doi:[10.1021/cr030063a](https://doi.org/10.1021/cr030063a)

- Chatterjee DK, Fong LS, Zhang Y (2008) Nanoparticles in photodynamic therapy: an emerging paradigm. *Adv Drug Deliv Rev* 60(15):1627–1637. doi:[10.1016/j.addr.2008.08.003](https://doi.org/10.1016/j.addr.2008.08.003)
- Cheong SK, Krishnan S, Cho SH (2009) Modeling of plasmonic heating from individual gold nanoshells for near-infrared laser-induced thermal therapy. *Med Phys* 36(10):4664–4671. doi:[10.1118/1.3215536](https://doi.org/10.1118/1.3215536)
- Cherukuri P, Glazer ES, Curley SA (2010) Targeted hyperthermia using metal nanoparticles. *Adv Drug Deliv Rev* 62(3):339–345. doi:[10.1016/j.addr.2009.11.006](https://doi.org/10.1016/j.addr.2009.11.006)
- Cinta S, Vogel E, Maniu D, Aluas M, Iliescu T, Cozar O, Kiefer W (1999) SERS mechanisms of the vitamin PP on different Au and Ag surfaces. *J Mol Struct* 482–483(1–3):679–684. doi:[10.1016/S0022-2860\(99\)00024-1](https://doi.org/10.1016/S0022-2860(99)00024-1)
- Corma A, Garcia H (2008) Supported gold nanoparticles as catalysts for organic reactions. *Chem Soc Rev* 37(9):2096–2126. doi:[10.1039/B707314N](https://doi.org/10.1039/B707314N)
- De-Llanos R, Sánchez-Cortes S, Domingo C, García-Ramos JV, Sevilla P (2011) Surface plasmon effects on the binding of antitumoral drug emodin to bovine serum albumin. *J Phys Chem C* 115(25):12419–12429. doi:[10.1021/jp111683c](https://doi.org/10.1021/jp111683c)
- Dulkeith E, Niedereichholz T, Klar TA, Feldmann J, von Plessen G, Gittins DI, Mayya KS, Caruso F (2004) Plasmon emission in photoexcited gold nanoparticles. *Phys Rev B* 70(20):205424. doi:[10.1103/PhysRevB.70.205424](https://doi.org/10.1103/PhysRevB.70.205424)
- Eby DM, Schaeublin NM, Farrington KE, Hussain SM, Johnson GR (2009) Lysozyme catalyzes the formation of antimicrobial silver nanoparticles. *ACS Nano* 3(4):984–994. doi:[10.1021/mn900079e](https://doi.org/10.1021/mn900079e)
- Edwards-Jones V (2009) The benefits of silver in hygiene, personal care and healthcare. *Lett Appl Microbiol* 49(2):147–152. doi:[10.1111/j.1472-765X.2009.02648.x](https://doi.org/10.1111/j.1472-765X.2009.02648.x)
- Elswaifi SF, Palmieri JR, Hockey KS, Rzigalinski BA (2009) Antioxidant nanoparticles for control of infectious disease. *Infect Disord Drug Targets* 9(4):445–452. doi:[10.2174/187152609788922528](https://doi.org/10.2174/187152609788922528)
- Epps DE, Rub TJ, Canola V, Chari A, Zamia M (1998) Determination of the affinity of drugs toward serum albumin by measurement of the quenching of the intrinsic tryptophan fluorescence of the protein. *J Pharm Pharmacol* 51(1):41–48. doi:[0.1211/0022357991772079](https://doi.org/10.1211/0022357991772079)
- Fasciani C, Bueno Alejo CJ, Grenier M, Netto-Ferreira JC, Scaiano JC (2011) High-temperature organic reactions at room temperature using plasmon excitation: decomposition of dicumyl peroxide. *Org Lett* 13(2):204–207. doi:[10.1021/ol1026427](https://doi.org/10.1021/ol1026427)
- Garcia AM, Alarcon E, Munoz M, Scaiano JC, Edwards AM, Lissi EA (2011) Photophysical behavior and photodynamic activity of zinc phthalocyanines associated to liposomes. *Photochem Photobiol Sci* 10(4):504–514. doi:[10.1039/C0PP00289E](https://doi.org/10.1039/C0PP00289E)
- Gebauer JS, Malissek M, Simon S, Knauer SK, Maskos M, Stauber RH, Peukert W, Treuel L (2012) Impact of the nanoparticle-protein corona on colloidal stability and protein structure. *Langmuir* 28(25):9673–9679. doi:[10.1021/la301104a](https://doi.org/10.1021/la301104a)
- Harmatz D, Blauer G (1975) Optical properties of bilirubin-serum albumin complexes in aqueous solution. A comparison among albumins from different species. *Archives of Biochemistry and Biophysics* 170(2):375–383. doi:[10.1016/0003-9861\(75\)90132-0](https://doi.org/10.1016/0003-9861(75)90132-0)
- Herne TM, Ahern AM, Carrel RL (1991) Surface-enhanced Raman spectroscopy of peptides: preferential N-terminal adsorption on colloidal silver. *J Am Chem Soc* 113(3):846–854. doi:[10.1021/ja00003a018](https://doi.org/10.1021/ja00003a018)
- Holland JT, Lau C, Brozik S, Atanassov P, Banta S (2011) Engineering of glucose oxidase for direct electron transfer via site-specific gold nanoparticle conjugation. *J Am Chem Soc* 133(48):19262–19265. doi:[10.1021/ja2071237](https://doi.org/10.1021/ja2071237)
- Honore B, Brodersen R (1984) Albumin binding of anti-inflammatory drugs. Utility of a site oriented versus a stoichiometric analysis. *Mol Pharmacol* 25(1):137–150
- Humphrey W, Dalke A, Schulten K (1996) VMD: visual molecular dynamics. *J Mol Graph* 14(1):33–38. doi:[10.1016/0263-7855\(96\)00018-5](https://doi.org/10.1016/0263-7855(96)00018-5)
- Jockusch S, Landis MS, Freiermuth B, Turro NJ (2001) Photochemistry and photophysics of α -hydroxy ketones. *Macromolecules* 34(6):1619–1626. doi:[10.1021/ma01836p](https://doi.org/10.1021/ma01836p)
- Kogan MJ, Bastus NG, Amigo R, Grillo-Bosch D, Araya E, Turiel A, Labarta A, Giralt E, Puntès VF (2006) Nanoparticle-mediated local and remote manipulation of protein aggregation. *Nano Lett* 6(1):100–115. doi:[10.1021/nl0516862](https://doi.org/10.1021/nl0516862)
- Kragh-Hansen U (1990) Structure and ligand binding properties of human serum albumin (review). *Dan Med Bull* 37(1):57–84
- Kubista M, Sojback R, Ericksson S, Albinsson B (1994) Experimental correction for the inner-filter effect in fluorescence spectra. *Analyst* 119(3):417–419. doi:[10.1039/AN9941900417](https://doi.org/10.1039/AN9941900417)
- Li WR, Xie XB, Shi QS, Zeng HY, Ou-Yang YS, Chen YB (2010) Antibacterial activity and mechanism of silver nanoparticles on *Escherichia coli*. *Appl Microbiol Biotechnol* 85(4):1115–1122. doi:[10.1007/s00253-009-2159-5](https://doi.org/10.1007/s00253-009-2159-5)
- Lynch I, Dawson KA (2008) Protein–nanoparticle interactions. *Nano Today* 3(1):40–47. doi:[10.1016/S1748-0132\(08\)70014-8](https://doi.org/10.1016/S1748-0132(08)70014-8)
- Mariam J, Dongre PM, Kothari DC (2011) Study of interaction of silver nanoparticles with bovine serum albumin using fluorescence spectroscopy. *J Fluoresc* 21(6):2193–2199. doi:[10.1007/s10895-011-0922-3](https://doi.org/10.1007/s10895-011-0922-3)
- Marin ML, McGilvray KL, Scaiano JC (2008) Photochemical strategies for the synthesis of gold nanoparticles from Au(III) and Au(I) using photoinduced free radical generation. *J Am Chem Soc* 130(49):16572–16584. doi:[10.1021/ja803490n](https://doi.org/10.1021/ja803490n)
- McEachran M, Kitaev V (2008) Direct structural transformation of silver platelets into right bipyramids and twinned cube nanoparticles: morphology governed by defects. *Chem Comm* 44:5737–5739. doi:[10.1039/B813519C](https://doi.org/10.1039/B813519C)
- McGilvray KL, Decan MR, Wang D, Scaiano JC (2006) Facile photochemical synthesis of unprotected aqueous gold nanoparticles. *J Am Chem Soc* 128(50):15980–15981. doi:[10.1021/ja066522h](https://doi.org/10.1021/ja066522h)
- Murawala P, Phadnis SM, Bhonde RR, Prasad BLV (2009) In situ synthesis of water dispersible bovine serum albumin capped gold and silver nanoparticles and their

- cytocompatibility studies. *Coll Surf B* 73(2):224–228. doi:[10.1016/j.colsurfb.2009.05.029](https://doi.org/10.1016/j.colsurfb.2009.05.029)
- Murphy CJ, Sau TK, Gole AM, Orendorff CJ, Gao J, Gou L, Hunyadi SE, Li T (2005) Anisotropic metal nanoparticles: synthesis, assembly, and optical applications. *J Phys Chem B* 109(29):13857–13870. doi:[10.1021/jp0516846](https://doi.org/10.1021/jp0516846)
- Nangia Y, Wangoo N, Goyal N, Suri CR (2009) A novel bacterial isolate *Stenotrophomonas maltophilia* as living factory for synthesis of gold nanoparticles. *Microb Cell Fact* 8(1):39–46. doi:[10.1186/1475-2859-8-39](https://doi.org/10.1186/1475-2859-8-39)
- Nayac NC, Shin K (2008) Human serum albumin mediated self-assembly of gold nanoparticles into hollow spheres. *Nanotechnology* 46(19):265603. doi:[10.1088/0957-4484/19/26/265603](https://doi.org/10.1088/0957-4484/19/26/265603)
- Pattabi RM, Pattabi M (2009) Synthesis and characterization of thiosalicylic acid stabilized gold nanoparticles. *Spect Acta: A* 74(1):195–199
- Peters T (1996) All about albumin proteins: biochemistry, genetics and medical applications, 1st edn. Academic Press, New York
- Pinkerton TC, Koeplinger KA (1990) Determination of warfarin-human serum albumin protein binding parameters by an improved Hummel-Dreyer high-performance liquid chromatographic method using internal surface reversed-phase columns. *Anal Chem* 62(19):2114–2122. doi:[10.1021/ac00218a013](https://doi.org/10.1021/ac00218a013)
- Ravindran A, Singh A, Raichur AM, Chandrasekaran N, Mukherjee A (2010) Studies on interaction of colloidal Ag nanoparticles with Bovine serum albumin (BSA). *Coll Surf B* 76(1):32–37. doi:[10.1016/j.colsurfb.2009.10.005](https://doi.org/10.1016/j.colsurfb.2009.10.005)
- Raymond FC, Gerald GV, Alexander N (1967) Fluorescence decay times: proteins, coenzymes, and other compounds in water. *Science* 156(3777):949–951. doi:[10.1126/science.156.3777.949](https://doi.org/10.1126/science.156.3777.949)
- Richardson HH, Carlson MT, Tandler PJ, Hernandez P, Govorov AO (2009) Experimental and theoretical studies of light-to-heat conversion and collective heating effects in metal nanoparticle solutions. *Nano Lett* 9(3):1139–1146. doi:[10.1021/nl8036905](https://doi.org/10.1021/nl8036905)
- Sakai T, Alexandridis P (2005) Mechanism of gold metal ion reduction, nanoparticle growth and size control in aqueous amphiphilic block copolymer solutions at ambient conditions. *J Phys Chem B* 109(16):7766–7777. doi:[10.1021/jp046221z](https://doi.org/10.1021/jp046221z)
- Scaiano JC, Aliaga C, Maguire S, Wang D (2006) Magnetic field control of photoinduced silver nanoparticle formation. *J Phys Chem B* 110(26):12856–12859. doi:[10.1021/jp061723t](https://doi.org/10.1021/jp061723t)
- Scaiano JC, Netto-Ferreira JC, Alarcon E, Billone P, Bueno Alejo CJ, Crites C-OL, Decan M, Fasciani C, González-Béjar M, Hallett-Tapley G, Grenier M, McGilvray KL, Pacioni NL, Pardoe A, René-Boisneuf L, Schwartz-Narbonne R, Silvero MJ, Stamplecoskie K, T-S W (2011) Tuning plasmon transitions and their applications in organic photochemistry. *Pure Appl Chem* 83(4):913–930. doi:[10.1351/PAC-CON-11-01-09](https://doi.org/10.1351/PAC-CON-11-01-09)
- Sharma VK, Yngard RA, Lin Y (2009) Silver nanoparticles: green synthesis and their antimicrobial activities. *Adv Coll Interf Sci* 145(1–2):83–96. doi:[10.1016/j.cis.2008.09.002](https://doi.org/10.1016/j.cis.2008.09.002)
- Shi X, Thomas TP, Myc LA, Kotlyar A, Baker JRJ (2007) Synthesis, characterization, and intracellular uptake of carboxyl-terminated poly(amidoamine) dendrimer-stabilized iron oxide nanoparticles. *Phys Chem Chem Phys* 9(42):5712–5720. doi:[10.1039/B709147H](https://doi.org/10.1039/B709147H)
- Slocik JM, Tam F, Halas NJ, Naik RR (2007) Peptide-assembled optically responsive nanoparticle complexes. *Nano Lett* 7(4):1054–1058. doi:[10.1021/nl070267x](https://doi.org/10.1021/nl070267x)
- Smith PK, Krohn RI, Hermanson GT, Mallia AK, Gartner FH, Provenzano MD, Fujimoto EK, Goeke NM, Olson BJ, Klenk DC (1985) Measurement of protein using bicinchoninic acid. *Anal Biochem* 150(1):76–85. doi:[10.1016/0003-2697\(85\)90442-7](https://doi.org/10.1016/0003-2697(85)90442-7)
- Stamplecoskie KG, Scaiano JC (2010) Light emitting diode irradiation can control the morphology and optical properties of silver nanoparticles. *J Am Chem Soc* 132(6):1825–1827. doi:[10.1021/ja910010b](https://doi.org/10.1021/ja910010b)
- Stamplecoskie KG, Scaiano JC, Tiwari VS, Anis H (2011) Optimal size of silver nanoparticles for surface-enhanced Raman spectroscopy. *J Phys Chem C* 115(5):1403–1409. doi:[10.1021/jp106666t](https://doi.org/10.1021/jp106666t)
- Suh JS, Moskovits M (1986) Surface-enhanced Raman spectroscopy of amino acids and nucleotide bases adsorbed on silver. *J Am Chem Soc* 108(16):4711–4718. doi:[10.1021/ja00276a005](https://doi.org/10.1021/ja00276a005)
- Sun Y, Xia Y (2002) Shape-controlled synthesis of gold and silver nanoparticles. *Science* 298(5601):2176–2179. doi:[10.1126/science.1077229](https://doi.org/10.1126/science.1077229)
- Swift J, Butts CA, Cheung-Lau J, Yerubandi V, Dmochowski IJ (2009) Efficient self-assembly of archaeoglobus fulgidus ferritin around metallic cores. *Langmuir* 25(9):5219–5225. doi:[10.1021/la8040743](https://doi.org/10.1021/la8040743)
- Tran ML, Centeno SP, Hutchison JA, Engelkamp H, Liang D, Van Tendeloo G, Sels BF, Hofkens J, Uji-i H (2008) Control of surface plasmon localization via self-assembly of silver nanoparticles along silver nanowires. *J Am Chem Soc* 130(51):17240–17241. doi:[10.1021/ja807218e](https://doi.org/10.1021/ja807218e)
- Triulzi RC, Dai Q, Zou J, Leblanc RM, Gu Q, Orbulescu J, Huo Q (2008) Photothermal ablation of amyloid aggregates by gold nanoparticles. *Colloids Surf B* 63(2):200–208. doi:[10.1016/j.colsurfb.2007.12.006](https://doi.org/10.1016/j.colsurfb.2007.12.006)
- Vamer KE, El-Badawy A, Feldhake D, Venkatapathy R (2010) State-of-the-science review: everything nanosilver and more. U.S. Environmental Protection Agency, Washington, DC. EPA/600/R-10/084
- Wadhwa S, Paliwal R, Paliwal SR, Vyas SP (2009) Nanocarriers in ocular drug delivery: an update review. *Curr Pharm Dess* 15(23):2724–2750. doi:[10.2174/12724](https://doi.org/10.2174/12724)
- Wikler MA (2005) Performance standards for antimicrobial susceptibility testing : fifteenth informational supplement, vol 25. Clinical and Laboratory Standards Institute, Wayne Pa, USA
- Wu Q, Cao H, Luan Q, Zhang J, Wang Z, Warner JH, Watt AAR (2008) Biomolecule-assisted synthesis of water-soluble silver nanoparticles and their biomedical applications. *Inorg Chem* 47(13):5882–5888. doi:[10.1021/ic8002228](https://doi.org/10.1021/ic8002228)
- Xiao Q, Huang S, Qi ZD, Zhou B, He ZK, Liu Y (2008) Conformation, thermodynamics and stoichiometry of HSA adsorbed to colloidal CdSe/ZnS quantum dots. *Biochim Biophys Acta* 1784(7–8):1020–1027. doi:[10.1016/j.bbap.2008.03.018](https://doi.org/10.1016/j.bbap.2008.03.018)